

Wavelet-based Temporal Attention Improves Traffic Forecasting

Yash Jakhmola¹, Nitish Kumar Mishra¹, Kripabandhu Ghosh¹, and Tanujit Chakraborty^{2,3}

¹ Indian Institute of Science, Education and Research, Kolkata, West Bengal, India
{y20ms028,nkm19ms127,kripaghosh}@iiserkol.ac.in

² Sorbonne University, Abu Dhabi, UAE

³ Sorbonne Center for Artificial Intelligence, Paris, France
tanujit.chakraborty@sorbonne.ae

Abstract. Spatio-temporal forecasting of traffic flow data represents a typical problem in the field of machine learning, impacting urban traffic management systems. Traditional statistical and machine learning methods cannot adequately handle both the temporal and spatial dependencies in these complex traffic flow datasets. A prevalent approach in the field is to combine graph convolutional networks and multi-head attention mechanisms for spatio-temporal processing. This paper proposes a wavelet-based temporal attention model, namely a wavelet-based dynamic spatio-temporal aware graph neural network (W-DSTAGNN), for tackling the traffic forecasting problem. Benchmark experiments using several statistical metrics confirm that our proposal efficiently captures spatio-temporal correlations and outperforms ten state-of-the-art models on three different real-world traffic datasets. Our proposed ensemble data-driven method can handle dynamic temporal and spatial dependencies and make long-term forecasts in an efficient manner.

Keywords: Traffic forecasting, Wavelet transformation, Temporal attention, Spatio-temporal data

1 Introduction

Spatio-temporal graph data are omnipresent in today’s world, with applications in various domains ranging from sensor networks [24,33] and climate modeling [14,18] to traffic control systems [6,12,30]. Among these, the traffic flow prediction datasets collected by California Transportation Agencies’ (CalTrans) Performance Measurement System (PeMS) became the most popular dataset for spatio-temporal forecasting since the traffic at each point is a function of highly dynamic temporal and spatial patterns. For example, traffic flow is affected by the time of the day we are considering - traffic can be high near residential areas during evening office closure times or near a school during the school opening times. Traffic can also be affected by nearby traffic conditions - if a road has very low traffic (perhaps due to some construction work), the traffic might be higher

on nearby roads. Moreover, all these patterns can change depending upon the day - traffic near schools and offices will be much less on weekends, while traffic near malls and shopping complexes will be higher on weekends, and vice-versa. These dynamic patterns make traffic flow prediction a very complicated task [1].

Previous studies focused on developing data-centric methods to tackle the challenges of traffic data. Classical time series analysis ranging from the autoregressive integrated moving average (ARIMA) model to the multivariate vector autoregression (VAR) model has been deployed for traffic forecasting tasks [23,5]. However, these models failed to capture the spatio-temporal correlation due to their incapability to handle the non-stationary complexities of the time sequences. Recently, deep learning models have been successfully applied to traffic forecasting problems. For example, an encoder-decoder architecture (both with spatial and temporal attention) along with a transform attention layer between the encoder and decoder, namely graph multi-attention network (GMAN), has been proposed [32]. Dynamic spatio-temporal aware graph neural network (DSTAGNN) [12] has been one of the recent state-of-the-art models for traffic forecasting due to its ability to handle the high-dimensional spatio-temporal nature of the traffic flow datasets. However, it fails to generate long-term forecasts and capture the seasonal patterns in the temporal structures of the PeMS traffic flow data.

Several decomposition techniques have shown competencies in time series pre-processing tasks, such as Fourier transforms [25], Fast Fourier transforms [7], and Wavelet decomposition [17], among many others. A recent study by [20] has shown that when a wavelet-transformed sequence is fed into a transformer (and then inverse transformed after), it improves the performance of the transformer for temporal forecasting of long-sequence data. To overcome the issues with DSTAGNN and other spatio-temporal forecasting models for traffic data, we introduce wavelet-based temporal attention to effectively model temporal dynamics and spatial patterns of PeMS datasets. Our proposed method (W-DSTAGNN) can simultaneously handle the non-stationarity and nonlinear structure of the spatio-temporal data and has the ability to generate long-term forecasts for the traffic data. In addition to this, our proposal, combined with conformal prediction, can generate prediction intervals for probabilistic forecasting of traffic flow data, which will be of immense use for traffic management systems. Our contributions can be summarized as follows:

1. We propose a novel framework that combines maximal overlapping discrete wavelet transformation (MODWT) and the temporal attention module (W-DSTAGNN) for learning long-term temporal and spatial dependencies of traffic conditions.
2. The proposed W-DSTAGNN (detailed in Section 4) captures the nonlinearity, non-stationarity, and complicated relations between the nodes in a better way than the standard traffic forecasting models. This is confirmed by large-scale experiments with three datasets (see section 5.1) and ten baselines (see section 5.3).

- Multiple comparisons with the best (MCB) test are performed to show that our model indeed performs better than the baselines (details in Section 5.4). We also presented a conformal prediction plot to give further evidence for the competence of our method in generating prediction intervals.

2 Related Work

With the number of vehicles on the road increasing every year, it is no surprise that current traffic management systems need to get even more effective. Traffic flow prediction plays an important role in such systems [1]; however, predicting traffic flow is not a trivial task. Traditional methods, like ARIMA [3], support vector regression (SVR) [9], and VAR [10], imposed strong stationarity assumptions and also only take temporal information into account. FC-LSTM [27], though very popular for sequence-to-sequence tasks, again struggles to take spatial information into account. It is challenging to accommodate complex spatial dependencies in these traditional statistical and machine learning approaches.

In recent years, many deep learning techniques have been employed to tackle the problem of high-dimensional spatio-temporal traffic prediction. Convolutional neural networks (CNNs) have been used in traffic forecasting due to their powerful capability in spatial information extraction; for example, [31] converts the road network to a regular 2D grid and applies CNN to predict the flow. Nowadays, graph convolutional networks (GCNs) are used to model spatial correlations in network data [4], which put spectral graph theory into deep neural networks. In another recent work, [8] proposed ChebNet, which boosts GCNs with fast localized convolution filters. More recently, diffusion convolutional recurrent neural network (DCRNN) [13] introduces graph convolutional networks into spatio-temporal network data prediction, which employs a diffusion graph convolution network to understand the information diffusion process in spatial networks, along with RNN to model temporal correlations. Spatio-temporal synchronous graph convolutional network (STSGCN) [26] concatenated the spatial graphs of multi-neighborhood time steps. Graph-WaveNet (GWN) [29] designed a self-adaptive matrix to understand the changes of the influence between nodes and their neighbors. It used dilated casual convolutions for the temporal correlations, thus increasing the receptive field exponentially. Adaptive graph convolutional recurrent network (AGCRN) [2] found hidden spatial dependencies via learnable embedding from nodes. However, the spatio-temporal layers cannot be stacked to expand the receptive field. GMAN [32] is an encoder-decoder architecture with spatial and temporal attention modules in both the encoder and decoder to model spatio-temporal correlations. It also has a transform attention layer between the encoder and decoder to alleviate error propagation during long-term prediction. Thus, the traffic flow prediction problem is an emerging research area for both transportation research and machine learning communities working on spatio-temporal data structures. A highly accurate traffic forecasting system impacts our day-to-day life. Our proposed methodology can serve as a long-term forecasting tool for traffic data modelers.

3 Mathematical Preliminaries

3.1 Wavelet Transformation

Wavelet is a ‘small’ wave-like oscillation, which is defined as a square-integrable function $\phi : \mathbb{R} \rightarrow \mathbb{R}$ such that $\int_{-\infty}^{\infty} \phi = 0$ and $\int_{-\infty}^{\infty} \phi^2 = 1$. The second condition ensures that the wavelet is ‘localized’ in time, thus allowing it to capture both the time and frequency of a signal, unlike the Fourier transform, which is capable of capturing only the frequency of the signal. A wavelet transform converts a time series into a sequence of time-indexed observations, with each time series representing the original data in a particular frequency band. The wavelet transform can be done in two ways - continuous wavelet transform (CWT), which applies every possible wavelet to the original series, and discrete wavelet transform (DWT), which applies a finite number of wavelets at a specific time and location. In this study, we utilize the DWT approach that represents a series using an orthonormal basis and is widely used in hydrology [19], epidemics [15], geophysics [20], and economics [22], among others. The DWT uses a dyadic grid. For scale parameter i and shift parameter k , the equation for the decompositions using DWT is

$$c(i, k) := \sum_t U(t)(2^{\frac{i}{2}}\Psi(2^i t - k))$$

where the sum is over the entire time series, U is the original time series (or signal), and Ψ is a mother wavelet.

3.2 Maximal Overlap Discrete Wavelet Transform (MODWT)

Application of DWT requires the sample size to be exactly a power of 2. Thus, a modified version of the DWT, namely maximal overlap discrete wavelet transform (MODWT), is adopted for decomposing arbitrary time series [16]. Both MODWT and DWT can accomplish multi-resolution analysis - a scale-based additive decomposition. However, in contrast to the usual DWT, in the MODWT, both wavelet and scaling coefficients are shift-invariant. Thus, circularly shifting the time series by any amount will circularly shift the MODWT details and smooth coefficients by a corresponding amount. This property is crucial, as it allows for the attention modules to be subjected to relatively ‘smoother’ data, which makes it easier for them to capture the underlying pattern. Also, contrary to the DWT details and smooth, the MODWT details and smooth are associated with zero-phase filters, thus allowing the extraction of true signal from noise in a multiresolution analysis of the original time series. This allows for each of the attention blocks to have meaningful weights associated with them, thus leading to a robust framework [16].

To find the MODWT coefficients of level j ($l = 1, 2, \dots, J$), the DWT coefficients are scaled and convolved with the original time series as follows:

$$D_{j,t} = \sum_{l=0}^{L_j-1} \frac{d_{j,l}}{2^{j/2}} U_{(t-l) \bmod M'} \quad S_{j,t} = \sum_{l=0}^{L_j-1} \frac{s_{j,l}}{2^{j/2}} U_{(t-l) \bmod M'}$$

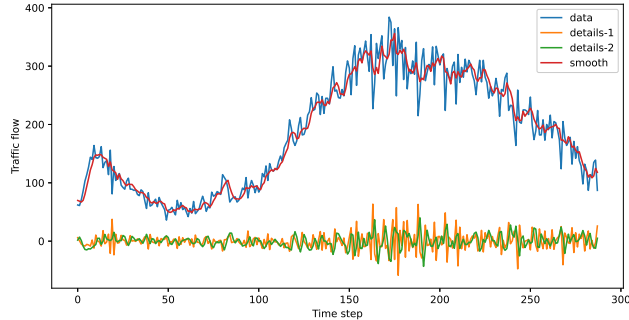


Fig. 1: Data and all MODWT coefficients (level 2, haar filter) for Day 1, Node 1 of PeMS04 dataset.

where $d_{j,l}, s_{j,l}$ are the details and scaling coefficients of DWT and $L_j = (2^j - 1)(L - 1) + 1$. Note that all the wavelet coefficients will have the same length as the original time series. Thus, the coefficients can be expressed in a matrix notation as

$$D_j = d_j U, \quad S_j = s_j U,$$

where d_j and s_j are square matrices of order M' consists of the wavelet and scaling filters respectively. Hence, using MODWT, the original time series U can be represented as

$$U = \sum_{j=1}^J d_j^T D_j + S_J^T S_J = \sum_{j=1}^J \tilde{D}_j + \tilde{S}_J,$$

where $\tilde{D}_j; j = 1, 2, \dots, J$ indicates the j^{th} level high frequency details and \tilde{S}_J represents the low frequency trend components. For a graphical illustration of the MODWT approach, we present the MODWT wavelet and scaling coefficients obtained by applying the transformation with the Haar filter at level 2 ($J = 2$) on a selected PeMS04 dataset in Figure 1.

4 Proposed Methodology: W-DSTAGNN

The wavelet dynamic spatio-temporal aware graph neural network (W-DSTAGNN) architecture consists of stacked spatio-temporal attention blocks with a MODWT transformation as a pre-processing step in the temporal module and a prediction layer. To initialize the spatio-temporal blocks, we design the traffic road network in a graphical manner such that each sensor acts as a node in the graph, and the edges represent the corresponding connections between the nodes. In the W-DSTAGNN architecture, we compute the spatial association among the nodes using spatio-temporal aware distance (STAD), as proposed in [12]. Thus the

$(i, j)^{th}$ entry of the adjacency matrix (A_{STAD}) based on STAD can be represented as $A_{STAD}[i, j] = 1 - d_{STAD}(i, j)$ with $d_{STAD}(i, j)$ being the STAD between the corresponding sensors. To ensure the sparsity level in the adjacency matrix, we set the sparsity hyperparameter $P_{sp} = 0.01$ such that for each node i ($i = 1, 2, \dots, N$), the number of non-zero elements is $N_r = N \times P_{sp}$ which has the maximum value. Thus, the spatio-temporal relevance graph (STRG) created using these sparse connections has the adjacency matrix $[A_{STRG}]_{N \times N}$ with only $N_r \times N_r$ non-zero elements. Along with STAD, we utilize the wavelet-based spatio-temporal attention block to capture the dynamic characteristics of the spatial dependencies with changes in time.

In the wavelet temporal attention (wTA) block, we first preprocess the data using the MODWT-based multiresolution analysis. Then, we use multi-head self-attention layers to capture the long-range correlation in the time series data. This enhances the effectiveness of modeling the dynamic temporal dependencies between the nodes. Thus, we first apply the MODWT transformation to the input $X^{(l)} \in \mathbb{R}^{N \times c^{(l)} \times M}$ and the residual attention from the previous layer $A^{(l-1)}$ to generate the corresponding details ($\tilde{D}_j^{X^{(l)}}; j = 1, 2, \dots, J$, $\tilde{D}_j^{A^{(l-1)}}; j = 1, 2, \dots, J$) and smooth ($\tilde{S}_j^{X^{(l)}}$, $\tilde{S}_j^{A^{(l-1)}}$) coefficients. In the W-DSTAGNN approach, we aim to apply temporal attention to $X^{(l)}, A^{(l-1)}$ by individually applying it to the details and smooth components and aggregating them using the inverse MODWT transformation. Thus, the wTA block can be mathematically represented as:

$$Y^{(l)} = \text{IMODWT} \left[f \left(\tilde{D}_1^{X^{(l)}}, \tilde{D}_1^{A^{(l-1)}} \right), \dots, f \left(\tilde{D}_J^{X^{(l)}}, \tilde{D}_J^{A^{(l-1)}} \right), f \left(\tilde{S}_J^{X^{(l)}}, \tilde{S}_J^{A^{(l-1)}} \right) \right],$$

where IMODWT is the Inverse MODWT, f is the temporal attention applied to the details and smooth coefficients, which is defined as follows ($f(\tilde{S}_J^{X^{(l)}}, \tilde{S}_J^{A^{(l-1)}})$ is defined in an analogous manner):

$$f \left(\tilde{D}_j^{X^{(l)}}, \tilde{D}_j^{A^{(l-1)}} \right) = \text{LayerNorm}(\text{FullyConnected}([\mathcal{O}^1, \dots, \mathcal{O}^H] + \tilde{D}_j^{X^{(l)}}))$$

where $\mathcal{O}^h := \text{softmax}(A^{(l)})V^{(l)}$, $\tilde{D}_j^{A^{(l)}} = \frac{Q^{(l)}K^{(l)T}}{\sqrt{d_H}} + \tilde{D}_j^{A^{(l-1)}}$, $d_H = \frac{d}{H}$, $Q^{(l)} := \tilde{D}_j^{X^{(l)}}W_q^{(l)}$, $K^{(l)} := \tilde{D}_j^{X^{(l)}}W_k^{(l)}$, $V^{(l)} := \tilde{D}_j^{X^{(l)}}W_v^{(l)}$ and $\tilde{D}_j^{X^{(l)}} \in \mathbb{R}^{c^{l-1} \times M \times N}$ is just a reshape of $\tilde{D}_j^{X^{(l)}} \in \mathbb{R}^{N \times c^{l-1} \times M}$, where M is the number of time steps, c^{l-1} is the feature dimension from the $(l-1)^{th}$ layer of the spatio-temporal block, and N is the number of nodes. The spatial attention (SA) module receives $Y^{(l)}$ as the input and applies the self-attention mechanism to compute the dynamic spatial dependencies. Mathematically, the attention output \mathcal{P} generated by the SA blocks can be represented as $\mathcal{P} = \text{SA}(Y^{(l)}) = [\mathcal{P}^1, \dots, \mathcal{P}^H]$ with

$$\mathcal{P}^h = \text{softmax} \left(\frac{(Y_E W_k^{(h)})(Y_E W_q^{(h)})}{\sqrt{d_H}} + W_m^{(h)} \odot A_{STRG} \right); h = 1, 2, \dots, H,$$

where $Y_E = \text{Embedding}(\text{Conv}(Y^*))$ and $Y^* \in \mathbb{R}^{c^{l-1} \times N \times M}$ is the transpose of $Y^{(l)}$ from the wTA layer. Thus, the output $\mathcal{P} = [\mathcal{P}^1, \mathcal{P}^2, \dots, \mathcal{P}^H]$ denotes the

spatio-temporal dynamic dependencies obtained by aggregating the output of the spatio-temporal attention modules.

The output of the wavelet spatio-temporal attention module is then passed into the spatial convolution block, which is a standard spatial graph convolution module that performs graph convolution based on Chebyshev polynomial approximation using the STAG. It is responsible for making complete use of the topological characteristics of the traffic network and learning the structure-aware node features.

$$Z^{(l)} = g_\theta *_G X^{(l)} = g_\theta(L)X^{(l)} = \sum_{k=0}^K \theta_k(T_k(\tilde{L}) \odot P^{(k)})X^{(l)},$$

where θ is learnable, $\tilde{L} := \frac{2}{\lambda_{max}}(D - A_{STAG}) - \mathbb{I}_N$, D is the diagonal matrix with $D_{ii} = \sum_j A_{STAG}(i, j)$, λ_{max} is the largest eigenvalue of $L = D - A_{STAG}$ and T_k is the k^{th} order Chebyshev polynomial. We finally process the output from the spatial layer using a temporal-gated convolutional network.

We use the temporal gated convolution layer, which is composed of three Gated Tanh Units (GTU) with different receptive fields. The forecast can be obtained as $X^{(l+1)} = \text{LayerNorm}(\text{ReLU}(X^{(l)} + Z_{out}))$ with

$$Z_{out} = \text{ReLU}(\text{Concat}(\text{Pooling}(\Gamma_1 *_\tau Z^{(l)}), \text{Pooling}(\Gamma_2 *_\tau Z^{(l)}), \text{Pooling}(\Gamma_3 *_\tau Z^{(l)})) + Z^{(l)})$$

where Γ_i is the convolution kernel of size s_i , $\Gamma *_\tau Q = \tanh(E) \odot \sigma(F)$ where E, F are the first and second halves of Q with respect to the channel dimension and concatenation and pooling is done such that $\frac{3M - (s_1 + s_2 + s_3 - 3)}{W} = M$. A pictorial illustration of the W-DSTAGNN architecture is given in Figure 2.

5 Experimental Setup

5.1 Datasets

To empirically validate the performance of the W-DSTAGNN architecture, we conduct experiments on real-world traffic forecasting benchmark datasets acquired from the Caltrans PeMS. Our datasets include the PeMS-BAY dataset curated by [13], as well as the PeMS03 and PeMS04 datasets preprocessed by [26]. All traffic datasets are gathered in real-time from several monitoring sensors strategically positioned throughout the freeway system across all major metropolitan areas of California, USA. The PeMS-BAY dataset accumulates information from 325 sensors in the Bay area, covering a six-month timespan from January 1, 2017 to May 31, 2017. The sensor distribution for the PeMS-BAY dataset is visualized in Figure 3. For the PeMS03 dataset, 358 sensors were selected, and three months of data were collected from September 1, 2018 to November 30, 2018. For PeMS04, data from 307 selected sensors are collected for two months, spanning from January 1, 2018 to February 28, 2018. For all the datasets, aggregated traffic speed readings at 5-minute intervals are used in the experimental analysis. A summary of all datasets, including the number

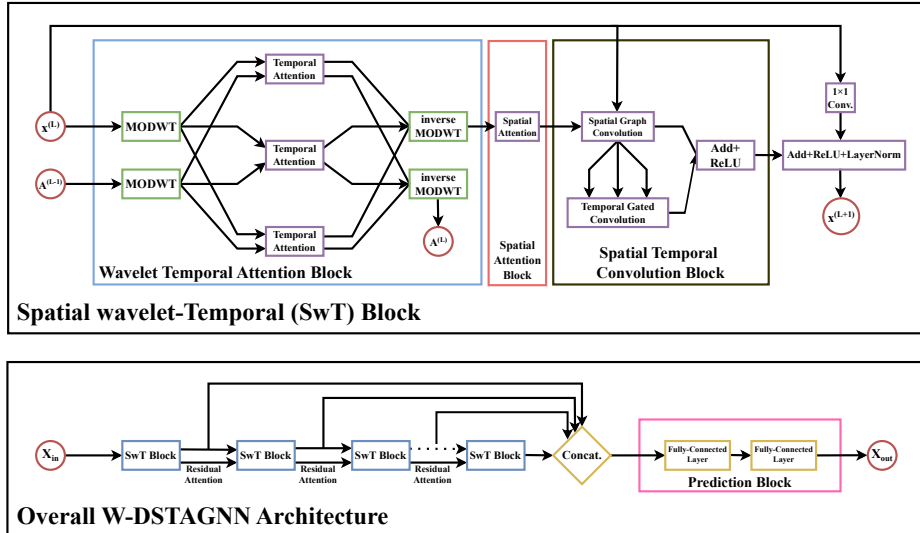


Fig. 2: Detailed framework of W-DSTAGNN

Table 1: Summary of the datasets

| Dataset | Nodes | Samples | Sample rate | Time Range |
|----------|-------|---------|-------------|-----------------------|
| PeMS-BAY | 325 | 52116 | 5 min | 01/01/2017-31/05/2017 |
| PeMS03 | 358 | 26209 | 5 min | 01/09/2018-30/11/2018 |
| PeMS04 | 307 | 16992 | 5 min | 01/01/2018-28/02/2018 |

of sensors (nodes), number of samples, sample rate, and time range, is provided in Table 1. For preprocessing the datasets, we apply normalization as $X_{normalized} = \frac{X - \text{mean}(X)}{\text{std}(X)}$ to ensure zero mean and unit variance before training our forecasting models. To check the stationarity of our datasets, we apply the Kwiatkowski–Phillips–Schmidt–Shin (KPSS) test and the Augmented Dickey–Fuller (ADF) test. The critical values of these statistical tests for a selected sensor are presented in Table 2. Overall, the test results depict that, according to the ADF test, all the time series corresponding to each sensor location for the PeMS-BAY, PeMS03, and PeMS04 datasets are stationary. However, according to the KPSS test, the time series corresponding to 246 sensors out of 325 for PeMS-BAY, 332 sensors out of 358 for PeMS03, and 298 sensors out of 307 for PeMS04 are stationary.

5.2 Performance measure

To measure the performance of different forecasting frameworks, we use three performance indicators, namely, mean absolute error (MAE), mean absolute percentage error (MAPE), and root mean squared error (RMSE). These metrics can be computed as: $MAE(x, \hat{x}) = \frac{1}{n} \sum_{i=1}^n |x_i - \hat{x}_i|$, $MAPE(x, \hat{x}) =$

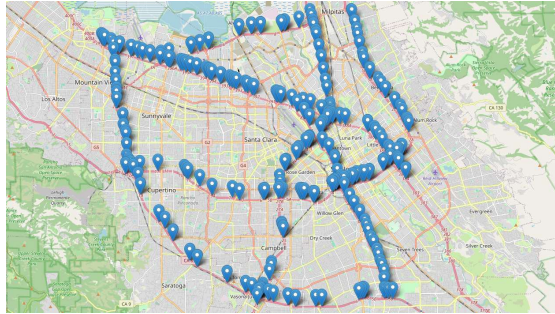


Fig. 3: Sensor distribution of PeMS-BAY dataset.

Table 2: ADF (Critical Value at 1% is -3.43) and KPSS (Critical Value at 10% is 0.35) test results for sensor number 38.

| Dataset | ADF Test Statistic | KPSS Test Statistic |
|----------|--------------------|---------------------|
| PeMS-BAY | -30.56 | 0.92 |
| PeMS03 | -15.81 | 0.07 |
| PeMS04 | -16.05 | 0.12 |

$\frac{1}{n} \sum_{i=1}^n \frac{|x_i - \hat{x}_i|}{x_i}$, $RMSE(x, \hat{x}) = \sqrt{\frac{1}{n} \sum_{i=1}^n (x_i - \hat{x}_i)^2}$ where $x = (x_1, \dots, x_n)$ is the testing data (ground truth), and $\hat{x} = (\hat{x}_1, \dots, \hat{x}_n)$ is the corresponding forecast. By general convention, the model with the least performance measure is the ‘best’ forecasting model. We reported the testing errors computed between the test data and the data forecasted by the model.

5.3 Baseline models

In this section, we briefly explain the baseline models used in our experimental analysis and discuss their implementation strategies as adopted from [13].

1. ARIMA (with Kalman filter) [3] is a well-known statistical model for time series forecasting. Implementation is done with orders (3,0,1) using the *statsmodel* [21] python package.
2. SVR [9] uses a linear support vector machine for regression. We use the penalty term $C = 0.1$ and the number of historical observations is 5 for the implementation.
3. VAR [10] is a linear forecasting technique that can model the pairwise relationships among time series. It is a modification of the ARIMA model for multivariate time series setup. Implementation is done by setting the number of lags to 3, using the *statsmodel* [21] python package.
4. FC-LSTM [27] is an encoder-decoder framework using LSTM with peephole. There are two recurrent layers in the encoder and the decoder. In each recurrent layer, there are 256 LSTM units. The L1 weight decay is $2e^{-5}$ and L2 weight decay is $5e^{-4}$. The batch size is 64, and the loss function is MAE.

The initial learning rate is $1e^{-4}$, which reduces by 1/10 every 10 epochs starting from the 20th epoch. Early stop is also performed by looking at the validation error.

5. DCRNN [13] integrates graph convolution into a gated recurrent unit. Implementation is adopted from the GitHub repository of [13].
6. STSGCN [26] includes local spatio-temporal subgraph modules and is implemented following the GitHub repository of [26].
7. GWN [29] integrates graph convolution with dilated casual convolution to understand spatio-temporal dependencies. This model is implemented using the code available at the GitHub repository of [29].
8. AGCRN [2] exploits learnable embedding of nodes in graph convolution. Implementation is adopted from the GitHub repository of [2].
9. GMAN [32] is a graph multi-attention network with spatial and temporal attention. We implemented this model using the GitHub repository of [32].
10. DSTAGNN [12] combines temporal and spatial attention with a graph convolutional network. Its implementation is adopted from the GitHub repository of [12].

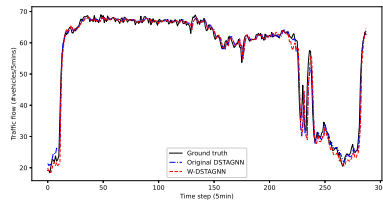
5.4 Experimental setup and performance comparison

In our experimental analysis, we segregate the datasets into training, validation, and test sets in the ratios 7:1:2 for PeMS-BAY data and 6:2:2 for the PeMS03 and PeMS04 datasets. To train the W-DSTAGNN model, we leverage the GPU of Google Colab Pro+. The implementation of the W-DSTAGNN architecture is done using the PyTorch library, and the source code for our model is made publicly available at <https://github.com/yash-jakhmola/w-dstagnn>. For certain baseline models, we use the forecasts reported in the seminal works of [26,13,12]. Table 3 shows the comparison of different approaches for forecasting 1-hour ahead traffic conditions. The proposed W-DSTAGNN consistently generates the best forecasts compared to the baseline models for two datasets, except for PeMS04. In PeMS04, W-DSTAGNN achieves the lowest RMSE score and performs similarly to DSTAGNN, as indicated by the MAPE values. In terms of the MAE metric, GMAN outperforms our proposal with a margin of 1.34%. For the univariate and the multivariate time-series models like ARIMA, SVR, VAR, and LSTM, their ability to capture only the temporal correlations, ignoring the spatial dependencies, led to their inferior performance. However, for the other spatio-temporal models, their better accuracy measures over the temporal architectures highlight the importance of modeling spatio-temporal dependencies. Moreover, as evident from Table 3, the proposed W-DSTAGNN architecture outperforms other models for most of the forecasting tasks. To emphasize the importance of wavelet transformation in the W-DSTAGNN model, we compare the performance improvement of W-DSTAGNN over standard DSTAGNN and report the results in Table 4. The values in Table 4 indicate percentage improvement in different metrics as computed using

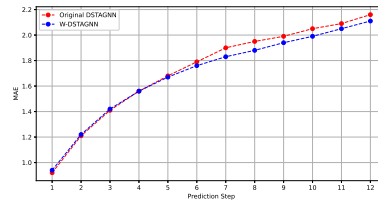
$$\frac{metric(DSTAGNN) - metric(W-DSTAGNN)}{metric(DSTAGNN)} \times 100\%.$$

Table 3: Experiment Results show that the proposed W-DSTAGNN model **outperforms** all baseline models.

| Baselines | PeMS-BAY | | | PeMS03 | | | PeMS04 | | |
|------------------|-------------|-------------|-------------|--------------|--------------|--------------|--------------|--------------|--------------|
| | MAE | MAPE(%) | RMSE | MAE | MAPE(%) | RMSE | MAE | MAPE(%) | RMSE |
| ARIMA [3] | 3.38 | 8.30 | 6.50 | 35.31 | 33.78 | 47.59 | 33.73 | 24.18 | 48.80 |
| SVR [9] | 3.28 | 8.00 | 7.08 | 21.97 | 21.51 | 35.29 | 28.70 | 19.20 | 44.56 |
| VAR [10] | 2.93 | 6.50 | 5.44 | 23.65 | 24.51 | 38.26 | 23.75 | 18.09 | 36.66 |
| FC-LSTM [27] | 2.37 | 5.70 | 4.96 | 21.33 | 22.33 | 35.11 | 26.24 | 19.30 | 40.49 |
| DCRNN [13] | 2.07 | 4.90 | 4.74 | 18.18 | 18.91 | 30.31 | 24.70 | 17.12 | 38.12 |
| STSGCN [26] | 2.11 | 4.96 | 4.85 | 17.48 | 16.78 | 29.21 | 21.19 | 13.90 | 33.65 |
| GWN [29] | 1.95 | 4.63 | 4.52 | 19.85 | 19.31 | 32.94 | 25.45 | 17.29 | 39.70 |
| AGCRN [2] | 1.96 | 4.64 | 4.54 | 15.98 | 15.23 | 28.25 | 19.83 | 12.97 | 32.26 |
| GMAN [32] | 1.86 | 4.31 | 4.32 | 16.87 | 18.23 | 27.92 | 19.14 | 13.19 | 31.60 |
| DSTAGNN [12] | 1.72 | 3.92 | 3.88 | 15.57 | 14.68 | 27.21 | 19.30 | 12.70 | 31.46 |
| W-DSTAGNN | 1.70 | 3.86 | 3.88 | 15.31 | 14.49 | 26.59 | 19.40 | 12.70 | 31.28 |



(a) 1st testing day, node 17 of PeMS-BAY



(b) PeMS-BAY

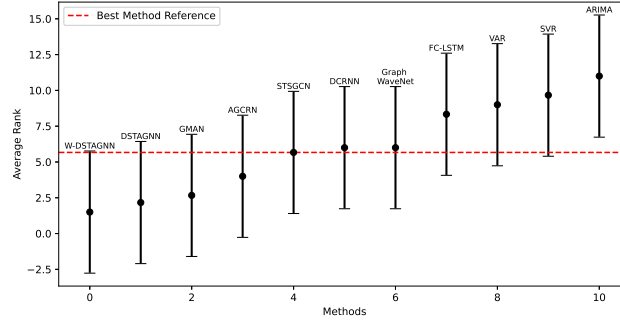
Fig. 4: Prediction Curve and MAE per prediction step plot.

It can be observed from the table that W-DSTAGNN improves the RMSE by a maximum of 2.28%, MAPE by 1.53%, and MAE by 1.67% of DSTAGNN. This improvement in the performance measures is primarily attributed to the use of MODWT decomposition in the DSTAGNN architecture, which helps segregate signals from noise in the input data. A higher node count allows for redundancies in the form of relations between the nodes, which do not get removed by MODWT. Thus, the temporal attention block is allowed to look for patterns in the transformed data, while the spatial attention is free to look into the intricate inter-node patterns that were missed by temporal attention, leading to better learning of the overall pattern in the dataset. A graphical illustration of the ground truth, along with the forecasts generated by the DSTAGNN and W-DSTAGNN for the first testing day of sensor 56 of PEMS-BAY, are presented in Figure 4a. Additionally, we present the MAE values of DSTAGNN and W-DSTAGNN models in each 5-minute interval for a 1-hour forecast period in Figure 4b.

Furthermore, to validate the statistical significance of our experimental evaluations, we used multiple comparisons with the best (MCB) test [11]. This non-

Table 4: Improvement(%) of W-DSTAGNN over DSTAGNN.

| Dataset | MAE | MAPE(%) | RMSE | Mean |
|----------|-------|---------|------|------|
| PeMS-BAY | 1.16 | 1.53 | 0 | 0.90 |
| PeMS03 | 1.67 | 1.29 | 2.28 | 1.75 |
| PeMS04 | -0.52 | 0 | 0.57 | 0.02 |

Fig. 5: MCB plot for MAE, $\alpha = 0.038$.

parametric test ranks the models based on their relative performance in terms of a specific metric and computes the corresponding critical distances. Figure 5 demonstrates the MCB plot for the MAE metric. This plot highlights that our proposal is the ‘best’ performing model as it achieves the minimum average rank (black dot) followed by other spatio-temporal architectures. Moreover, the maximum value of the critical distance of the W-DSTAGNN (black line) represents the reference value of the test (red dotted line). Since the critical distance of the ARIMA model lies well above the reference value, we can conclude that its performance is significantly inferior to the W-DSTAGNN model.

5.5 Hyperparameter Tuning

To ensure a fair comparison between the W-DSTAGNN and DSTAGNN approaches, we utilize similar hyperparameters for both models. However, W-DSTAGNN includes an additional hyperparameter indicating the level of MODWT decomposition. If the level is large, more temporal attention blocks need to be trained. However, MODWT also reduces the number of epochs needed to train the model. Table 5 reports the performance metrics of W-DSTAGNN computed for different levels (up to 3) of MODWT decomposition. As evident from the table, level 2, with two detail components and a smooth series, performs best in terms of all metrics for all datasets except for the RMSE of PeMS-BAY, which is inferior to level 1 by 0.26%.

Table 5: Hyperparameter tuning results. It can be seen that level 2 gives the best results.

| Level | PeMS-BAY | | | PeMS03 | | | PeMS04 | | |
|-------|-------------|-------------|-------------|--------------|--------------|--------------|--------------|--------------|--------------|
| | MAE | MAPE(%) | RMSE | MAE | MAPE(%) | RMSE | MAE | MAPE(%) | RMSE |
| 1 | 1.70 | 3.88 | 3.87 | 15.53 | 14.51 | 26.96 | 19.45 | 12.89 | 31.33 |
| 2 | 1.70 | 3.86 | 3.88 | 15.31 | 14.49 | 26.59 | 19.40 | 12.70 | 31.28 |
| 3 | 1.72 | 4.01 | 3.96 | 15.62 | 14.83 | 27.29 | 19.56 | 12.96 | 31.28 |

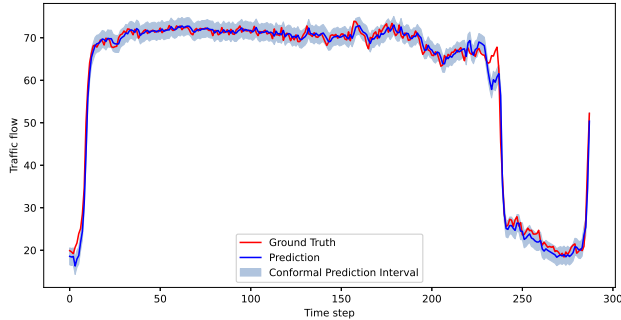


Fig. 6: 90% conformal prediction plot for first testing day, node 56 of PeMS-BAY

5.6 Conformal Predictions

Along with the point estimates, we provide conformal predictions for a selected testing day of the PeMS-BAY dataset in Figure 6 to quantify the 90% uncertainty associated with our framework. The conformal prediction approach translates point estimates into prediction regions in a distribution-free, model-agnostic manner, guaranteeing convergence [28]. To compute these prediction intervals, we find the residuals of the trained model applied to a calibration (validation) set. Then, we compute the nonconformity scores by calculating the absolute difference between the true and predicted values and finding the α^{th} quantile (d) of these scores. The conformal prediction interval for a test sample y is thus given by $[y - d, y + d]$. Our conformal prediction restricts data leakage and generates reliable prediction intervals because modeling uncertainties are done using the validation data.

6 Conclusion

In this paper, we presented a spatio-temporal deep learning model to perform traffic forecasting integrating wavelet decomposition with a temporal attention mechanism. Our ensemble approach outperformed other state-of-the-art models on these real-world datasets, specifying their potential to tour spatio-temporal

structures from the input time series. The key advantage of our proposed W-DSTAGNN method is its capacity to generate accurate and reliable long-term forecasts of traffic flows and prediction intervals for business deployment. We tested our method using statistical tests to verify its robustness over benchmark models. An immediate extension of our proposed approach would be to explore other potential application areas, such as spatio-temporal predictions of epidemics or studying the evolving behavior of social networks.

References

1. Ayözen, Y.E., İnaç, H.: Traffic planning in modern large cities paris and istanbul. *Scientific reports* **14**(1), 1–10 (2024)
2. Bai, L., Yao, L., Li, C., Wang, X., Wang, C.: Adaptive graph convolutional recurrent network for traffic forecasting. *Advances in neural information processing systems* **33**, 17804–17815 (2020)
3. Box, G.E., Jenkins, G.M., Reinsel, G.C., Ljung, G.M.: *Time series analysis: forecasting and control*. John Wiley & Sons (2015)
4. Bruna, J., Zaremba, W., Szlam, A., LeCun, Y.: Spectral networks and locally connected networks on graphs. arXiv preprint arXiv:1312.6203 (2013)
5. Chandra, S.R., Al-Deek, H.: Predictions of freeway traffic speeds and volumes using vector autoregressive models. *Journal of Intelligent Transportation Systems* **13**(2), 53–72 (2009)
6. Choi, J., Choi, H., Hwang, J., Park, N.: Graph neural controlled differential equations for traffic forecasting. In: *Proceedings of the AAAI conference on artificial intelligence*. vol. 36, pp. 6367–6374 (2022)
7. Cochran, W.T., Cooley, J.W., Faviv, D.L., Helms, H.D., Kaenel, R.A., Lang, W.W., Maling, G.C., Nelson, D.E., Rader, C.M., Welch, P.D.: What is the fast fourier transform? *Proceedings of the IEEE* **55**(10), 1664–1674 (1967)
8. Defferrard, M., Bresson, X., Vandergheynst, P.: Convolutional neural networks on graphs with fast localized spectral filtering. *Advances in neural information processing systems* **29** (2016)
9. Drucker, H., Burges, C.J., Kaufman, L., Smola, A., Vapnik, V.: Support vector regression machines. *Advances in neural information processing systems* **9** (1996)
10. Hamilton, J.D.: *Time series analysis*. Princeton university press (2020)
11. Koning, A.J., Franses, P.H., Hibon, M., Stekler, H.O.: The m3 competition: Statistical tests of the results. *International journal of forecasting* **21**(3), 397–409 (2005)
12. Lan, S., Ma, Y., Huang, W., Wang, W., Yang, H., Li, P.: Dstagnn: Dynamic spatial-temporal aware graph neural network for traffic flow forecasting. In: *International conference on machine learning*. pp. 11906–11917. PMLR (2022)
13. Li, Y., Yu, R., Shahabi, C., Liu, Y.: Diffusion convolutional recurrent neural network: Data-driven traffic forecasting. arXiv preprint arXiv:1707.01926 (2017)
14. Mei, J., Moura, J.M.: Signal processing on graphs: Estimating the structure of a graph. In: *2015 IEEE International Conference on Acoustics, Speech and Signal Processing (ICASSP)*. pp. 5495–5499. IEEE (2015)
15. Panja, M., Chakraborty, T., Kumar, U., Liu, N.: Epicasting: an ensemble wavelet neural network for forecasting epidemics. *Neural Networks* **165**, 185–212 (2023)
16. Percival, D.B., Mofjeld, H.O.: Analysis of subtidal coastal sea level fluctuations using wavelets. *Journal of the American Statistical Association* **92**(439), 868–880 (1997)

17. Percival, D.B., Walden, A.T.: Wavelet methods for time series analysis, vol. 4. Cambridge university press (2000)
18. Ray, A., Chakraborty, T., Ghosh, D.: Optimized ensemble deep learning framework for scalable forecasting of dynamics containing extreme events. *Chaos: An Interdisciplinary Journal of Nonlinear Science* **31**(11) (2021)
19. Sang, Y.F.: A review on the applications of wavelet transform in hydrology time series analysis. *Atmospheric research* **122**, 8–15 (2013)
20. Sasal, L., Chakraborty, T., Hadid, A.: W-transformers: a wavelet-based transformer framework for univariate time series forecasting. In: 2022 21st IEEE international conference on machine learning and applications (ICMLA). pp. 671–676. IEEE (2022)
21. Seabold, S., Perktold, J.: Statsmodels: econometric and statistical modeling with python. *SciPy* **7**, 1 (2010)
22. Sengupta, S., Chakraborty, T., Singh, S.K.: Forecasting cpi inflation under economic policy and geo-political uncertainties. arXiv preprint arXiv:2401.00249 (2023)
23. Shahriari, S., Ghasri, M., Sisson, S., Rashidi, T.: Ensemble of arima: combining parametric and bootstrapping technique for traffic flow prediction. *Transportmetrica A: Transport Science* **16**(3), 1552–1573 (2020)
24. Shi, X., Feng, H., Zhai, M., Yang, T., Hu, B.: Infinite impulse response graph filters in wireless sensor networks. *IEEE Signal Processing Letters* **22**(8), 1113–1117 (2015)
25. Sneddon, I.N.: Fourier transforms. Courier Corporation (1995)
26. Song, C., Lin, Y., Guo, S., Wan, H.: Spatial-temporal synchronous graph convolutional networks: A new framework for spatial-temporal network data forecasting. In: Proceedings of the AAAI conference on artificial intelligence. vol. 34, pp. 914–921 (2020)
27. Sutskever, I., Vinyals, O., Le, Q.V.: Sequence to sequence learning with neural networks. *Advances in neural information processing systems* **27** (2014)
28. Vovk, V., Gammerman, A., Shafer, G.: Algorithmic learning in a random world, vol. 29. Springer (2005)
29. Wu, Z., Pan, S., Long, G., Jiang, J., Zhang, C.: Graph wavenet for deep spatial-temporal graph modeling. arXiv preprint arXiv:1906.00121 (2019)
30. Yu, B., Yin, H., Zhu, Z.: Spatio-temporal graph convolutional networks: A deep learning framework for traffic forecasting. arXiv preprint arXiv:1709.04875 (2017)
31. Zhang, J., Zheng, Y., Qi, D., Li, R., Yi, X., Li, T.: Predicting citywide crowd flows using deep spatio-temporal residual networks. *Artificial Intelligence* **259**, 147–166 (2018)
32. Zheng, C., Fan, X., Wang, C., Qi, J.: Gman: A graph multi-attention network for traffic prediction. In: Proceedings of the AAAI conference on artificial intelligence. vol. 34, pp. 1234–1241 (2020)
33. Zhu, X., Rabbat, M.: Graph spectral compressed sensing for sensor networks. In: 2012 IEEE International Conference on Acoustics, Speech and Signal Processing (ICASSP). pp. 2865–2868. IEEE (2012)